

Airfoils at High Angles of Attack using Synthetic Jets

Catalin Nae, Ph.D.

National Institute of Aerospace Research

B-dul Pacii no. 220, sect 6, code 7738

Bucharest, ROMANIA

Abstract

Some numerical results are presented for the case of the NACA 0012 airfoil having arrays of synthetic jets on the lower and the upper side. The analysis is using an unsteady Navier – Stokes code modified in order to impose blowing conditions on the airfoil. For small incidences, results are compared with existing reference data. At high angles of attack, the results are compared with stalling characteristics of the non-blowing case. Several blowing regimes, with peak blowing velocity and frequency, were investigated. Flowfield spectra of the interaction of the jets and the boundary layer are presented. Results prove that synthetic jets can be used in order to improve stalling behaviour and pitch control. Also, a noise reduction analysis might be considered by controlling the local pressure distribution in the leading edge zone.

Introduction

Synthetic jets result from an oscillating diaphragm in an enclosed space, having small orifices at the top(Fig. 3). Several such devices may be considered in the form of an array acting independently or as a single unit, and being incorporated in an airfoil in several location on the upper or the lower side. They can be controlled electrostatically or using piezoelectric materials with frequencies in the range of 0.5 – 20 KHz. Because air is drawn into the cavity by the low-level suction pressure created by the diaphragm and then is expelled by the same diaphragm, such devices are considered to produce a zero-mass jet. The peak velocity speed and the frequency are defining parameters. For practical devices with orifice diameters like 200 μm , peak velocity may be up to 20m/s, as reported in several experiments.

The numerical experiment

Such arrays of synthetic jets were assumed in different positions on the upper and the lower side of the NACA 0012 airfoil. Their presence was simulated in the form of an unsteady surface transpiration boundary condition in a Navier – Stokes code. Several test cases were considered for zero incidence and 5 deg. incidence. Results were compared with existing reference data obtained by Hassan and JanakiRam.

At high angles of attack, the same code, with special treatment of leading edge zone, was used. Global airfoil characteristics were computed and compared with reference data from wind tunnel experiments for the non-blowing case. Several cases were considered for the frequency and the peak velocity of the synthetic jets.

The 2D CFD code

The code used is of RANS type, based on a modified $k - \epsilon$ turbulence model. For this study, some modifications of the initial version were made.

The code is based on a combination of finite-volume and finite-element method, using general unstructured meshes. Due to the difficulty in obtaining reliable unstructured meshes by the Delaunay-Voronoi method (for blowing cases, the first grid points off the airfoil were located at $1.0e-05$), some elliptic grids were used, converted to a triangular mesh by natural triangularization.

The Navier-Stokes and the k-ε equations are solved using a finite volume (Galerkin) upwind technique using a Roe solver for the convective part of the system. The viscous part is solved using a typical centered Galerkin technique.

The global formulation used is:

$$\frac{\partial}{\partial t}(W) + \nabla \cdot F(W) = \nabla \cdot N(W) \quad \text{where :}$$

$$W = \begin{pmatrix} \rho \\ \rho \cdot U \\ \rho \cdot V \\ \rho \cdot E \\ \rho \cdot k \\ \rho \cdot \varepsilon \end{pmatrix} \quad F_x(W) = \begin{pmatrix} \rho \cdot U \\ \rho \cdot U^2 + p \\ \rho \cdot U \cdot V \\ (\rho \cdot E + p) \cdot U \\ \rho \cdot U \cdot k \\ \rho \cdot U \cdot \varepsilon \end{pmatrix} \quad F_y(W) = \begin{pmatrix} \rho \cdot V \\ \rho \cdot U \cdot V \\ \rho \cdot V^2 + p \\ (\rho \cdot E + p) \cdot V \\ \rho \cdot V \cdot k \\ \rho \cdot V \cdot \varepsilon \end{pmatrix}$$

$$N_x(W) = \begin{pmatrix} 0 \\ \tau_{xx} \\ \tau_{xy} \\ \kappa_{tot} \cdot \frac{\partial}{\partial x} T + U \cdot \tau_{xx} + V \cdot \tau_{xy} \\ (\mu + \mu_t) \cdot \frac{\partial}{\partial x} k \\ (\mu + C_\varepsilon \cdot \mu_t) \cdot \frac{\partial}{\partial x} \varepsilon \end{pmatrix} \quad N_y(W) = \begin{pmatrix} 0 \\ \tau_{xy} \\ \tau_{yy} \\ \kappa_{tot} \cdot \frac{\partial}{\partial x} T + U \cdot \tau_{xy} + V \cdot \tau_{yy} \\ (\mu + \mu_t) \cdot \frac{\partial}{\partial y} k \\ (\mu + C_\varepsilon \cdot \mu_t) \cdot \frac{\partial}{\partial y} \varepsilon \end{pmatrix}$$

$$\begin{aligned} \tau_{xx} &= \mu_{tot} \cdot \left(2 \cdot \frac{\partial}{\partial x} U - \frac{2}{3} \cdot \nabla \cdot u \right) \\ \tau_{xy} &= \mu_{tot} \cdot \left(\frac{\partial}{\partial y} U + \frac{\partial}{\partial x} V \right) \\ \tau_{yy} &= \mu_{tot} \cdot \left(2 \cdot \frac{\partial}{\partial y} V - \frac{2}{3} \cdot \nabla \cdot u \right) \end{aligned} \quad \text{and} \quad \begin{aligned} \nabla \cdot u &= \frac{\partial}{\partial x} U + \frac{\partial}{\partial y} V \\ \mu_{tot} &= \mu + \mu_t \\ \kappa_{tot} &= \mu \cdot \frac{\gamma}{Pr} + \mu_{tot} \cdot \frac{\gamma}{Pr_t} \end{aligned}$$

The steady state solution is obtained using an iterative scheme. The algorithm is explicit in time. It was found that a four stage Runge-Kutta scheme is the best choice :

$$\frac{\partial}{\partial t} W = \text{RHS}(W) \quad \text{and} \quad \begin{aligned} W^0 &= W^n \\ W^i &= W^0 + \alpha_k \cdot \Delta t \cdot \text{RHS}(W^{i-1}) \quad i = 1 \dots k \\ W^{n+1} &= W^k \end{aligned}$$

An important feature is the time step strategy. The following formula was used in order to compute the local time step at a given node.

$$\Delta t(P_i) = \min \left(\frac{\Delta x}{|u| + c}, \frac{1}{2} \cdot \rho \cdot Pr \cdot \frac{\Delta x^2}{\mu + \mu_t} \right)$$

For steady state computation, a local time step strategy was used. For unsteady cases, the global time step was used, as the minimum time step of all local computed time steps using the formula above.

The turbulence model used is based on the k - ε model. Due to the large amount of turbulent kinetic energy that is dissipated on the upper side of the airfoil close to the leading edge, some important features were used. This is the global approach used :

- A box of approx. 5% of the chord length was defined around the leading edge of the airfoil
- A box surrounding the array of synthetic jets on the lower side of the airfoil was defined
- A two layer k-ε model was used, based on the Reynolds number.
- A point checking routine was used in order to solve the viscous part of the NS system

The high Reynolds model is a commonly used one (2 equations).

The low Reynolds model is different for the regions defined on the airfoil. For the leading edge box, the low Reynolds model is using wall laws technique. In this way, the amount of kinetic turbulent energy dissipated in this region is reduced. The low Reynolds model is also used in the case of blowing, in the corresponding box. For the rest of the airfoil, the low Reynolds model used is based on the one-equation model defined by Mohammadi. The coupling with the high Reynolds model is made using a local Reynolds number value of 200.

Results for the non-blowing case at a stalling point are presented in Fig. 1 for the flowfield spectra. Lift history for the same case is presented in Fig. 5.

The synthetic jets simulation

An array of synthetic jets was defined on the lower side of the airfoil. The extend of this array was between 10% to 20% of the airfoil length, starting at 10% from the leading edge. The blowing law used was :

$$V_b = V_0 * \sin(2\pi f_b t)$$

All values used were normalised by the free stream speed of sound. Also, there was no phase shift for the blowing/suction activity, all jets having the instantaneous speed given by the above formula. Also, all computations were started from an initial viscous solution, corresponding to the no-blowing case.

In order to have an comparison criteria, the simulations were first made for the cases presented by Hassa and JanakiRam (Mach = 0.6, Reynolds = 3 million, NACA 0012). Here are some results for CL:

V_0	f_b	Alpha	CL_{ref}	CL
0.1	1585	0.0	0.16	0.1655
0.2	1585	0.0	0.38	0.3836
0.2	3170	0.0	0.33	0.3150
0.2	1585	5.0	0.81	0.8217

Some results for the blowing case at zero angle of attack are presented in Fig.2 .

A complex analysis was then performed for the case of the NACA 0012 at Mach = 0.248, Reynolds = 1.8 million. Results were compared with a reference for the non-blowing case. For the case presented in Fig. 4, the synthetic jets array was on the lower side of the airfoil, starting at 10% from the leading edge, the peak velocity was 0.2 at a frequency of 3200 Hz.

Some results and conclusions

The numerical analysis showed some important aspects of the synthetic jets on airfoils. Here are some of the most important ones :

- At relative small angles of attack, synthetic jets may be used for lift improvement. They have to be used on the lower side of the airfoil, starting around 10% from the leading edge, on around 10% in the chord length.
- At higher incidences, due to the grow of the y-component of the free stream velocity, the blowing peak velocity is decreasing, even changing sign at higher angles. The result is that blowing is less effective and even has a negative effect on the lift characteristics.
- The lower lift characteristics at high angles of attack are compensated by the shape of the lift curve. This is a sign of a delayed stall situation that can be controlled by the blowing regime.
- Lift characteristics, combined with drag and pitch, show that synthetic jets can be used as an alternative to the classical control devices.
- If noise is an important design factor, then using synthetic jets for pressure control on the leading edge might be a solution.
- More numerical simulations are required in order to investigate the interaction of several arrays of synthetic jets located on both the lower and the upper side of the airfoil.

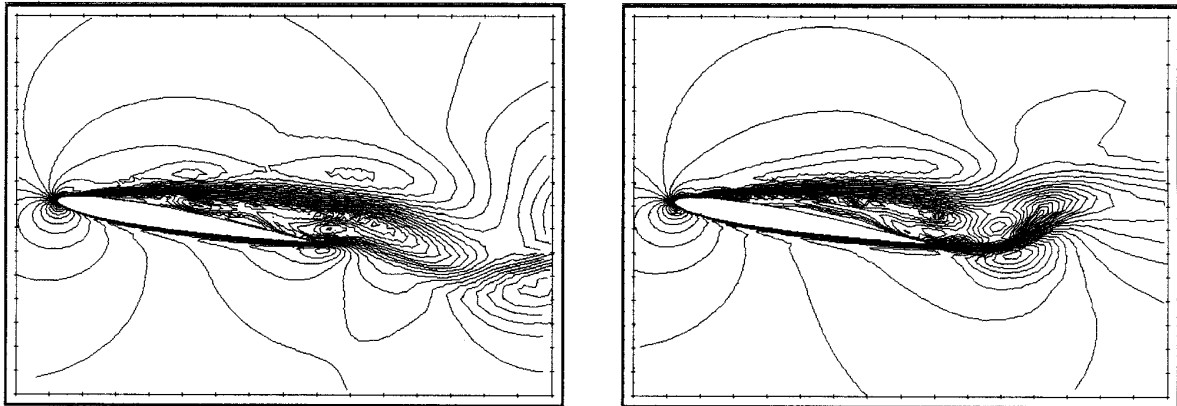


Fig. 1 Mach contours ($\alpha = 13^\circ$, no blowing, unsteady)

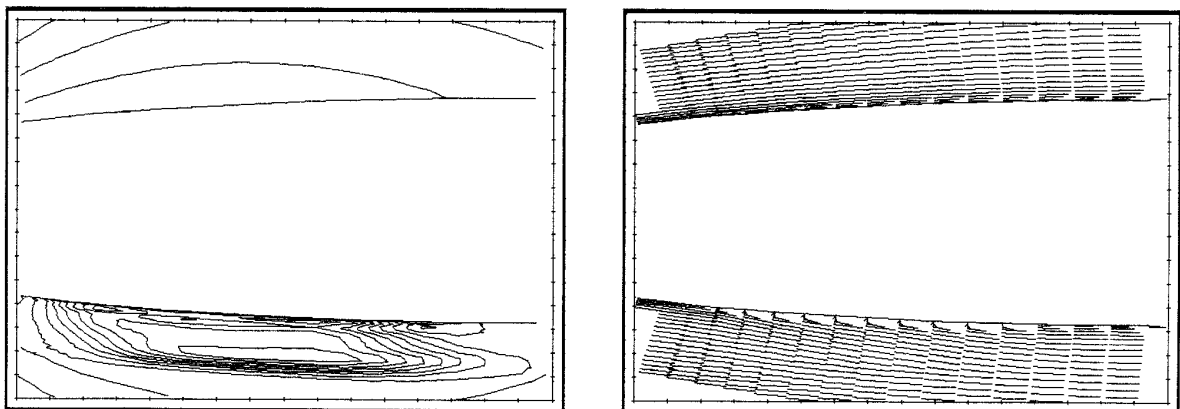


Fig. 2 Pressure contours and velocity profile ($\alpha = 0^\circ$, blowing)

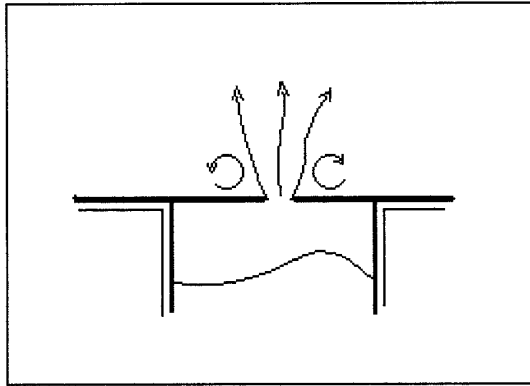


Fig. 3 Synthetic jet schematic representation

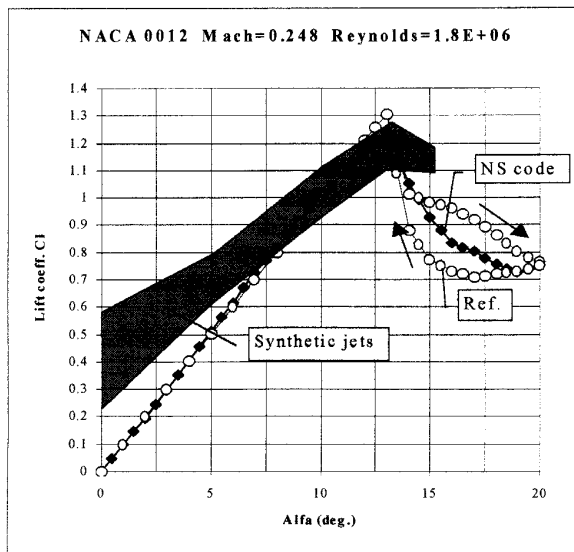


Fig 4 Synthetic jets effect

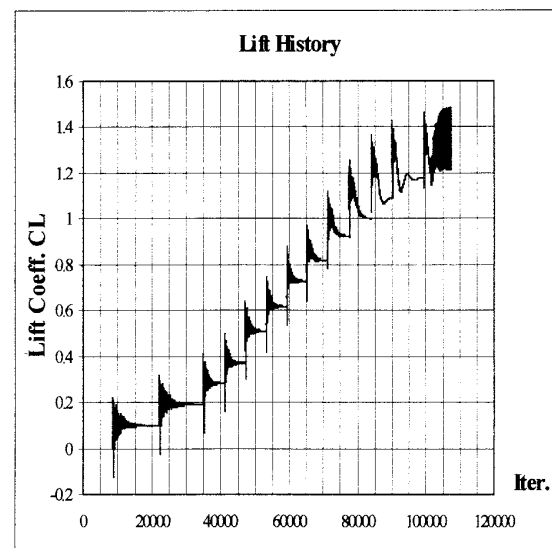


Fig. 5 Lift history (no blowing)